SCIENTIFIC REPORTS

OPEN

SUBJECT AREAS:
BIOSENSORS
BIOMATERIALS
CANCER IMAGING
BIOMARKERS

Received
7 November 2012

Accepted
11 December 2012

Published
29 January 2013

Correspondence and requests for materials should be addressed to X.W. (xuewang@seu.edu.cn)

In vivo self-bio-imaging of tumors through *in situ* biosynthesized fluorescent gold nanoclusters

Jianling Wang[1], Gen Zhang[1], Qiwei Li[1], Hui Jiang[1], Chongyang Liu[3], Christian Amatore[2] & Xuemei Wang[1]

[1]State Key Laboratory of Bioelectronics (Chien-Shiung Wu Lab), School of Biological Science and Medical Engineering, Southeast University, Nanjing, 210096, China, [2]Ecole Normale Supérieure, UMR CNRS-ENS-UPMC 8640 and LIA CNRS XiamENS NanoBioChem Departement de Chimie, 24 rue Lhomond 75005 Paris (France), [3]Daping Hospital, Third Military Medical University, Chongqing, 400042, China.

Fluorescence imaging *in vivo* allows non-invasive tumor diagnostic thus permitting a direct monitoring of cancer therapies progresses. It is established herein that fluorescent gold nanoclusters are spontaneously biosynthesized by cancerous cell (i.e., HepG2, human hepatocarcinoma cell line; K562, leukemia cell line) incubated with micromolar chloroauric acid solutions, a biocompatible molecular Au(III) species. Gold nanoparticles form by Au(III) reduction inside cells cytoplasms and ultimately concentrate around their nucleoli, thus affording precise cell imaging. Importantly, this does not occur in non-cancerous cells, as evidenced with human embryo liver cells (L02) used as controls. This dichotomy is exploited for a new strategy for *in vivo* self-bio-imaging of tumors. Subcutaneous injections of millimolar chloroauric acid solution near xenograft tumors of the nude mouse model of hepatocellular carcinoma or chronic myeloid leukemia led to efficient biosynthesis of fluorescent gold nanoclusters without significant dissemination to the surrounding normal tissues, hence allowing specific fluorescent self-bio-marking of the tumors.

Cancer is still extremely difficult to treat, so effective diagnosis strategies in the early stages of cancer are critical. In this respect, imaging has become an indispensable tool in cancer clinical trials and medical practice. *In vivo* fluorescence imaging of tumors may offer a possibility for the direct bio-imaging of tumors for precise diagnosis of cancer and monitoring of the treatment process[1,2]. *In situ* fluorescent bio-imaging is also of great significance for visualizing the expression and activity of particular molecules, cells, and biological processes that influence the behavior of tumors and/or their responsiveness to therapeutic drugs[3]. Therefore, a wide range of fluorescent components have been explored in the *in vivo* bio-imaging study, including the bio-marking of tumor tissues[4], angiogenic vasculature[5], and sentinel lymph nodes[6]. In this respect, several kinds of nanomaterials such as quantum dots[2], noble metal nanoparticles[7], upconverted nanoparticles[8], and new hybrid nanocomposites of reduced graphene oxide and gold nanoparticles[9] have demonstrated great potential for highly sensitive optical imaging of cancer on both cellular and animal levels.

In this perspective, gold nanoclusters are novel promising biocompatible nanoprobes, offering surfaces and cores exhibiting physicochemical properties (e.g., optical chirality[10,11], fluorescence[12,13], near-infrared photoluminescence[12,14,15], ferromagnetism[16].) that will provide new opportunities for clinical diagnostics. As such, these materials will undoubtedly play a critical role in the early diagnosis and sensitive detection of cancer. This is, however, balanced by the difficulty of targeting nanoparticles towards one type of cell, and by the fact that nanoparticles are easily disseminated inside most cells. Even if, when injected intravenously, circulating nanoparticles may be transferred to tumors through pores created in blood capillaries in the vicinity of tumors[17], the fact remains that such nanoparticles will be readily recognized by the immune system, removed from circulation, and stored in the liver and kidneys, unless they are first capped with specific molecules.

To overcome this severe difficulty, herein we propose a different novel strategy that relies on the fact that cancer cells have a completely different redox homeostasis from normal cells. They spontaneously produce high quantities of oxidants (ROS and RNS, viz., reactive oxygen or nitrogen species), which could readily result in a large amount of longevity hydrogen peroxide. Since its abnormal overproduction is known to be implicated in the progress of inflammatory diseases[18], the high-sensitivity visualization of relevant hydrogen peroxide level *in vivo* is of clinical importance as a diagnostic imaging[19]. These peculiarities are exploited hereafter by providing cancer cells with an alternate biocompatible electron acceptor short-circuiting these mechanisms and forcing them to

biosynthesize *in situ* fluorescent gold nanoclusters inside their cytoplasms. The proof of concept of this novel strategy is established using chloroauric acid biocompatible salts. $HAuCl_4$ is shown to undergo a more rapid and efficient spontaneous reduction into gold nanoclusters inside cancerous cells than in normal ones, enabling self-bio-imaging of cancer cells and tumors by long-lasting fluorescent markers. This novel strategy is established *ex vivo* on two different cancerous cell lines, HepG2, from human hepatocarcinoma and K562, from leukemia and confirmed *in vivo* on xenograft tumor mouse models of hepatocellular carcinoma or chronic myeloid leukemia which result specifically marked in the presence of $HAuCl_4$. Reduction of $HAuCl_4$ does not occur with the same efficiency in non cancerous cells as evidenced by comparison normal embryo liver cells (L02 cells) and normal mouse model, which remain fluorescent-silent when submitted to the same incubation protocol with $HAuCl_4$. Since the fluorescent gold nanoclusters grow directly in tumor cells/tissues and remain sequestrated within, any side problems related to the dissemination of nanoparticles to surrounding normal cells/tissues/organs are prevented while they accumulate within the tumors. Furthermore, gold nanoclusters biosynthesized *in situ* from $HAuCl_4$ display fluorescent properties similar to those of chemically prepared gold nanoclusters, thus providing an excellent opportunity for *in vivo* imaging of tumors by laser confocal scanning microscopy and *in vivo* bio-imaging microscopy.

Results

Self-imaging of cancer cells based on *in situ* biosynthesized gold nanoclusters. The biosynthesis of metallic nanomaterials is currently being explored through the use of bacteria[20], yeast[21], fungi[22], plant biomass[23,24], or living plants and plant extracts[25,26]. All these processes enable the production of highly stable nanomaterials without the addition of any capping agents to prevent molecular aggregation[27]. The present *in situ* gold-nanocluster biosynthesis from Au(III) salts is thought to exploit the classical mechanisms of bio-mineralization of inorganic ions: sequestration and reduction followed by scaffolding by functional biomolecules to produce nanominerals (Fig. 1).

Two different cell lines (HepG2, human hepatocarcinoma; K562, leukemia) were selected as models to evaluate the pertinence of the strategy schematized in Fig. 1 in individual cells and tumors, respectively. In the case of HepG2 cells incubated with chloroauric acid solutions, scanning electron microscopy (SEM) (Fig. 2A), black or gray areas) showed that cells retained their shape and morphology. The EDS (energy dispersive X-ray spectroscopy) observation indicates that after HepG2 cells incubation with chloroautic acid solutions, the calculated atom content of Au reaches 0.66% (from a random region of 2 μm × 2 μm, Fig. 2A inset). Simultaneously, the oxygen and nitrogen contents are ca. 23.01% and 20.54%, respectively, which originate from the cells. It is evident that the significant quantity of gold nanoclusters could be obtained by *in situ* biosynthesis inside HepG2 cell cytoplasms. The absence of cytotoxicity of this protocol in cells was established by MTT assays (see Fig. S1 in Supplementary Information (SI)). The SEM images also demonstrated the presence of gold nanoclusters biosynthesized *in situ* (white spots indicated by the white arrows in Fig. 2 (B)) by HepG2 cells incubated with chloroauric acid solutions. It is noted that initially, large gold nanoclusters with a rather uniform size distribution could essentially be spotted by SEM near the cell membranes (Fig. 2B), but these were ultimately disseminated in the whole cell cytoplasm, as shown by fluorescence microscopy (Fig. 3A for HepG2; see Fig. S3 in SI for K562) and fluorescence tomography images (Fig. S2 in SI for HepG2). These observations prove that gold nanoclusters could readily be prepared by *in situ* biosynthesis in live tumor cells, offering a promising opportunity for *in vivo* bio-imaging applications.

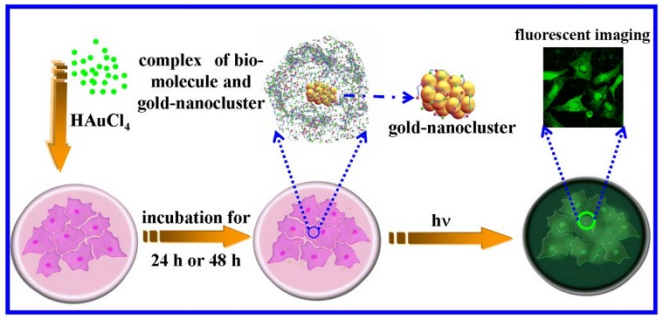

Figure 1 | Schematic illustration of *in situ* biosynthesis of gold nanoclusters in cells and tumor imaging. $HAuCl_4$ solution was incubated *in vitro* with target cells or subcutaneously injected *in vivo* near a tumor. The sequestration and reduction of $AuCl_4^-$ anions inside cells give rise to the progressive formation of gold nanoclusters. After incubation for 24–48 h, fluorescent gold nanoclusters were observed inside the tumor cells or accumulated around the tumor.

TEM analysis (Fig. S4 (A) in SI) established that 90% of the *in situ* biosynthesis gold nanoclusters ranged between 2–3 nm in diameter. HRTEM (Fig. S4 (A), inset) showed that the gold nanoclusters kept their interplanar Au–Au spacing at ~0.2 nm. To further confirm the formation of gold nanoclusters by *in situ* biosynthesis inside the cells, X-ray photoelectron spectroscopy (XPS) was used to investigate the valence of gold atoms in the gold nanoclusters after the reaction. As shown in Fig. S5, there were two peaks located at the binding energies of 84.15 and 87.53 eV, which was consistent with the emission of 4f photoelectrons from Au(0)[28], thereby suggesting the successful formation of gold nanoclusters.

Gold nanoparticle sols synthesized by chemical means exhibit a surface plasmon band giving rise to a broad absorption band in the visible region around 525 nm. This is in good agreement with our observation (Fig. S4 (B)) in which the present biosynthesized gold nanoparticles display the same typical UV/Vis absorption spectrum as observed for chemically prepared gold nanoclusters. In addition, the fluorescence of gold nanoclusters biosynthesized *in situ* could be observed clearly (Figs. 2–3 and Figs. S2–S3 in SI), which corresponded with the steady-state fluorescence spectrum of gold nanoclusters in aqueous solution with an emission peak at ca. 580 nm. Lin et al.[29] reported a quantum yield of 1.83 ± 0.32% for gold nanoclusters in water, thus placing them in a suitable range for applications in optical devices and biosensors.

The bright green fluorescence of gold nanoclusters biosynthesized *in situ* inside HepG2 and K562 cancer cells appears to be adequate for their use for *in vivo* bio-imaging of relevant live tumor cells. This is validated in Fig. 3 and Fig. S3 in SI, which also demonstrates that after incubation with 10 μM chloroauric acid solutions, a molecular Au(III) precursor, the gold nanoclusters biosynthesized in the cells were well distributed in the cells, so that the resulting edges and morphologies of the cells were neatly delineated. Importantly, the fluorescence intensity increased with incubation time, especially in the nucleoli regions (Fig. 3B). On the basis of the relative cellular fluorescence intensities, comparison between the fluorescence micrographs in Fig. 3A and Fig. 3B clearly demonstrates that the concentration of biosynthesized gold nanoclusters inside the cells not only increased with time in the cytoplasm, but also progressively settled inside or around the nucleoli at longer times, suggesting that the gold nanoclusters are biosynthesized in the cell cytoplasm and then migrate towards their nuclei. Raman spectroscopic investigations of HepG2 cells after 48 h-incubation with 10 μmol/L chloroauric acid solutions (see Fig. S6 in SI) evidenced that the biosynthesized gold nanoclusters interacted with biomolecules inside or around the nucleoli[9,30–33], giving rise to Raman enhanced effect spectroscopic bands. This confirmed the above fluorescence studies demonstrating that biosynthesized gold nanoclusters

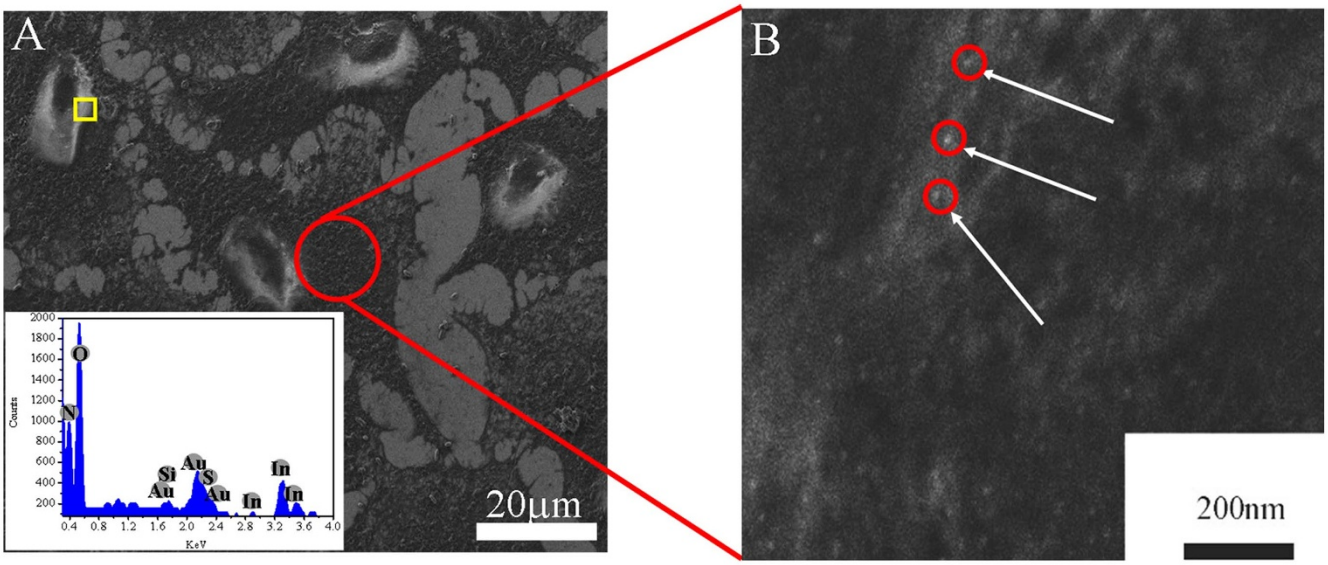

Figure 2 | Scanning electron microscopy (SEM) images of HepG2 cells after incubation with 10 μmol/L $HAuCl_4$ and biosynthesis of gold nanoclusters. (A) Panoramic images of HepG2 cells with gold nanoclusters; A inset: EDS of a rectangle region indicated by yellow border; (B) Enlarged SEM image illustrating the presence of gold nanoclusters (white spots indicated by white arrows). See SI for cell culture and incubation protocols.

progressively settled inside or around the nucleoli (Fig. 3B) involving close interactions with proteins and DNA[30–32].

Importantly, this biosynthesis of nanoparticles from chloroauric acid solutions seem specific to the cancerous cell model, since no formation of gold nanoparticles was observed in control experiments involving normal embryo liver cells (L02 cells). This is indicated in Figs. 3C and 3D, which show that there is no significant fluorescence for L02 cells subjected to the same incubation conditions as used for the HepG2 cells. This is further confirmed by a comparison of the quantitative variations in the fluorescence intensities across both cell types, as shown in Fig. 3E. Moreover, mounting evidence suggests that, compared with their normal counterparts, many types of cancer cells have increased levels of reactive oxygen species (ROS)[17,33,35]. Our recent quantitative evaluation of intracellular oxidative stress elicited by H_2O_2 of tumor cells also demonstrate the much higher level of H_2O_2 existing in different types of tumor cell lines (i.e., human leukemia cells K562, human hepatoma cell HepG2 and others) than those by normal cell lines. For example, the amount of H_2O_2 by hepatic tumor cells (HepG2) is ~25% higher than that of the normal hepatic cells (L02)[34]. Such high levels of ROS and RNS[35] involve at one stage or another reduction of dioxygen by specific enzymatic pools in order to recycle key reduced molecules produced by cells. When Au(III) salts are offered to the cells, these compete with the reduction of dioxygen. However, reduction of Au(III) into gold clusters of specific size (ca. 2 nm) requires in addition the presence of specific ligands prone to favor the gold species aggregation. For example, it is reported that hydroquinones, hydrogen peroxide[36] could act as such ligands, both species being present at higher levels in cancer cells than in normal ones. Hence, there are circumstances of established factors, which supply our present finding that cancer cells submitted to $HAuCl_4$ solution generate spontaneously gold clusters. Though, the exact metabolisms involved still needs to be established, which is far beyond the scope of this work.

***In vivo* self-bio-marking of tumors through biosynthesized gold nanoclusters.** The above results established the *ex-vivo* validity of the present approach, forcing these cancer cells to spontaneously produce and confine self-imaging fluorescent markers when incubated with chloroauric acid solutions. We now wish to establish the feasibility of *in vivo* bio-imaging of tumors by fluorescence based on *in situ* bio-synthesized fluorescent gold nanoclusters. For this purpose, we relied on a xenograft tumor model of hepatocellular carcinoma or chronic myeloid leukemia in nude mice (see SI for construction of the xenograft tumor mouse model). As shown in Fig. 4 and Fig. S7, subcutaneous injection of chloroauric acid solution around xenograft tumors allowed the clear observation of bright fluorescence around the tumor after 24 hours, while the control mouse was hardly observed by *in vivo* fluorescence imaging 48 h after a subcutaneous injection of 10 mmol/L $HAuCl_4$ solution in the right side of their abdomen (Fig. 4 (D)). After 72 hours, the fluorescence was still observable, though the fluorescence area was slightly extended, indicating that the biosynthesized gold nanoclusters diffused weakly around the tumor. No obvious toxic effects were observed over the experimental period, suggesting that chloroauric acid solutions could be administered *in situ*, and thus leading to long-lasting biosynthesized gold-nanocluster fluorescent labels for the *in vivo* self-bio-imaging of relevant tumors.

Discussion

Direct delivery to tumors remains a problem in most nanoparticle applications because the immune system rapidly removes circulating nanoparticles by ultimately accumulating them in the liver and kidneys. However, the present strategy eludes these mechanisms since it does not rely on injections of vectorized nanoparticles but proceeds through enforcing an efficient spontaneous reduction of a biocompatible molecular Au(III) precursor by cancer cells. Reduction of the molecular precursor inside the cancerous cells is presumably due to the reducing bio-agents, which allow the cells to control their inherent highly oxidized status[35,37]. The mechanism involved is still unclear. However, the fact that no nanocluster biosynthesis occurs in the normal cell controls or in normal tissues surrounding the xenograft tumors under the conditions and time periods considered here suggests that the mechanism must stem from some specific biochemical characteristics of tumor cells which differentiate them from cells under normal homeostatis[35,37]. It is already known that the tumor generated much more H_2O_2 than normal cell lines, as a result of an elevation of ROS production capacity in abnormal growth of tumor cells[38,39]. One may envision that since cancer cells generate high levels of reactive oxygen species through reduction of dioxygen, this peculiarity of cancer cells/tumor tissues can provide Au(III) salts

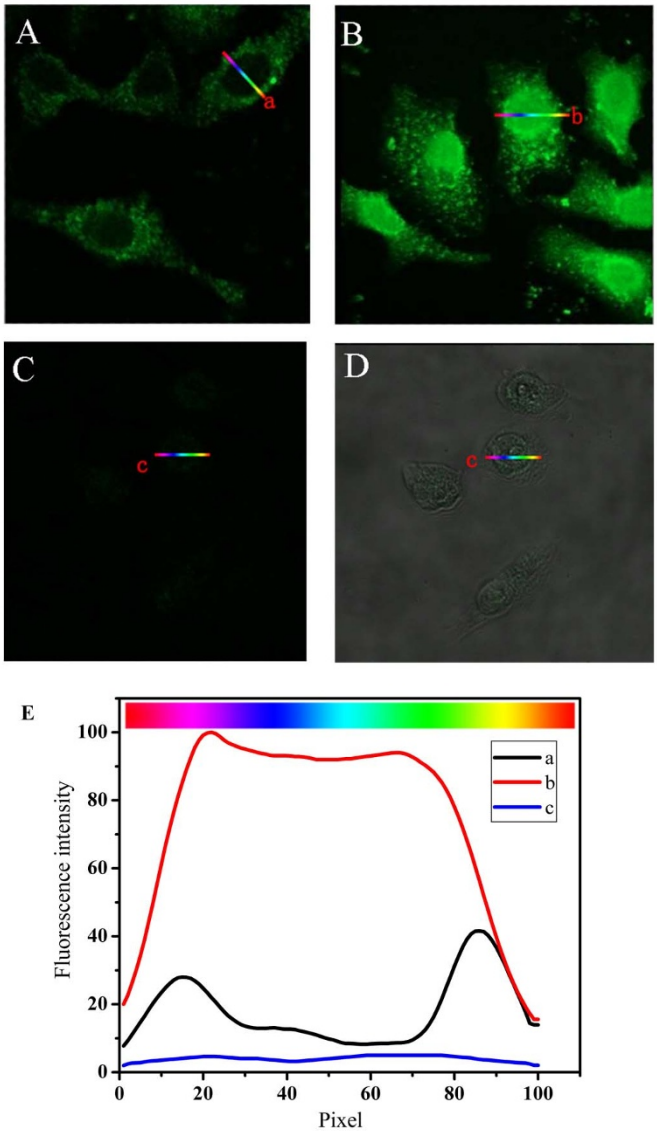

Figure 3 | Laser confocal fluorescence micrographs of HepG2 (A and B) and L02 control cells (C and D) incubated with identical 10 µmol/L $HAuCl_4$ solutions. A: after 24 h incubation; B, C and D: after 48 h incubation; D: Overlay of the morphological and fluorescence image of C. Images were acquired at 400-fold magnification. E: Relative fluorescence intensity variations along cross-sections a (in A), b (in B), or c (in C) (the color gradient coding illustrates the direction of the sampling). See SI for cell culture and incubation protocols and Fig. S3 for K562 cell lines.

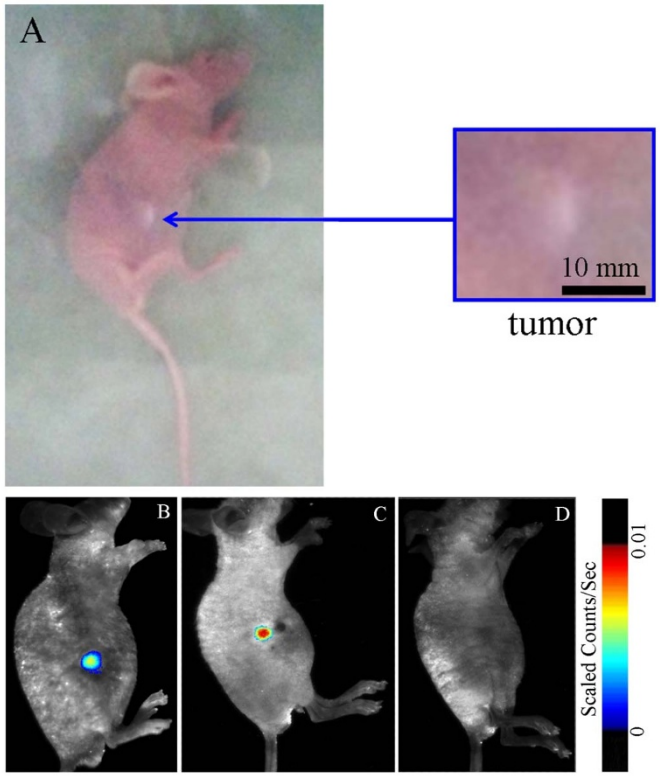

Figure 4 | Representative xenograft tumor mouse models of hepatocellular carcinoma observed in normal light (A) or by *in vivo* fluorescence imaging (B) 24 h after a subcutaneous injection of 10 mmol/L $HAuCl_4$ solution near the tumor. In (A), the inset shows an enlarged view of the xenograft tumor. Xenograft tumor mouse models of chronic myeloid leukemia observed by in vivo fluorescence imaging (C) 24 h after a subcutaneous injection of 10 mmol/L $HAuCl_4$ solution near the tumor. (D) Control mouse observed by in vivo fluorescence imaging 48 h after a subcutaneous injection of 10 mmol/L $HAuCl_4$ solution in the right side of their abdomen.

with an alternate electron donator to provoke an *in situ* biosynthesis of fluorescent gold nanoclusters in their cytoplasms.

Since noble metal-centered anions can cross outer bacteria membranes and react as electron acceptors in their inside[40,41], it is also plausible that at longer incubation $AuCl_4^-$ may disrupt several specific electron transfer chain pathways including those active in mitochondria. Indeed, the progressive dissemination of gold nanoclusters inside cells cytoplasms at longer incubation times (Figs. 3B, E, Fig. S3 in SI) may result from their simple migration from their biosynthesizing locations near cell membranes but also from a later but efficient activation of redox actors such as mitochondria which are distributed within cell cytoplasms. Though, it is clear from SEM images (Fig. 2B) and site mapping fluorescence (Fig. 3A, E, Figs. S2, S3 in SI) that the initial formation of gold nanoclusters occurs extremely close to cell membranes. Hence, enzymatic pools located here and highly active in cancer cells are certainly privileged actors in the reduction of Au(III) salts. In fact, this is precisely where important pools of NAD(P)H-oxidases and NO-synthases are located[35,37]. One may also consider that reduction of $AuCl_4^-$ anions disrupts defense pathways against oxidative stress such as that involving glutathione reductase[42] which catalyzes the NADPH-dependent reduction of oxidized glutathione[43].

All such routes are thermodynamically reasonable and may actually be competing synergistically for elimination of $AuCl_4^-$ anions which have penetrated inside cells depending on their individual kinetics and the access of $AuCl_4^-$ anions to electron donors and enzymatic catalysts[40,41,44]. Though, all these tentative mechanistic rationalizations involve molecular and enzymatic components present in target cells. So the dichotomous behavior observed here between normal and cancerous cells presumably reflects the fact that cancer cells may reduce Au(III) anions at sufficiently high rates for allowing Au(0) seeds to be formed, a fact which is perfectly compatible with their propensity to produce high ROS and RNS fluxes by reduction of dioxygen and resist against them[35,37,42,43].

Even though the exact mechanism(s) sustaining this novel self-imaging of cancer cells and tumors remain(s) unknown at this stage, this new strategy appears to be of great interest. Indeed, not only it specifically targets cancerous cells/tissues by forcing them to biosynthesize fluorescent gold nanoclusters inside their cytoplasm, but it also excludes the dissemination of the biosynthesized nanoparticles to adjacent normal cells/tissues since they remain mostly sequestrated in cell cytoplasms and cluster around or inside their nuclei.

Thus, this proof of concept opens up promising opportunities for biomedical applications requiring specific and sensitive imaging of tumors without direct injection of vectorized nanoparticles or molecular fluorescent probes.

Methods

Cell culture and cytotoxicity assessment. HepG2 cells (human hepatocarcinoma) and Leukemia K562 cells were purchased from Shanghai Institute of Cells, Chinese Academy of Sciences. L02 cells (human embryo liver cell strand) were obtained from Third Military Medical University (Chongqing, China).

HepG2 and L02 cells were maintained in DMEM (high glucose, Gibco) medium supplemented with 10% fetal calf serum (Sigma, USA), 100 U/mL penicillin (Sigma, USA), and 100 mg mL^{-1} streptomycin (Sigma, USA) at 37°C with 5% CO_2 in a 95% humidified atmosphere. The cell viability was measured by MTT assays. HepG2 cells in log phase were trypsinized and then seeded in 96-well plates. After 24 h resting time, each cell type was rinsed in DMEM and incubated with various concentrations of $HAuCl_4$ solution additions (0.0001, 0.001, 0.01, 0.1, 1.0 mmol/L) for 48 h. 3-(4,5)-dimethylthiahiazo (-z-y1)-3,5-di-phenytetrazoliumromide (MTT) solution was then added, and the cells were incubated for a further 4 h. DMSO was added to solubilize the formazan crystal, and OD 490 was recorded.

Leukemia K562 cells were maintained in RPMI 1640 (Gibco) medium supplemented with 10% fetal calf serum (Sigma, USA), 100 U/mL penicillin (Sigma, USA), and 100 mg mL^{-1} streptomycin (Sigma, USA) at 37°C with 5% CO_2 in a 95% humidified atmosphere.

Characterization of *in situ* biosynthesized gold nanoclusters. Gold nanoclusters were biosynthesized *in situ* through incubation of HepG2 or K562 cells with various concentrations of $HAuCl_4$ (Sigma Aldrich, USA) added to usual cells under culturing conditions. After 24 h or 48 h incubation, the presence of biosynthesized gold nanoclusters was characterized by UV-Vis-NIR , fluorescence spectroscopy, scanning electron microscopy (SEM) and transmission electron microscope (TEM). No formation of gold nanoclusters was observed in L02 control cells incubated with the same protocols.

UV-Vis absorption and fluorescence spectra were also measured from gold-nanocluster solutions extracted from incubated HepG2 cells by a repetitive freeze-thaw method, using a UV-Vis-NIR spectrophotometer (Shimadzu, UV3600), and a fluorescence spectrometer (PerkinElmer, LS-55), respectively. For Raman spectroscopy study, HepG2 cells were treated before and after incubation with 10 μmol/L $HAuCl_4$ for 48 h. An excitation wavelength at 532 nm, 50% laser intensity, and overlaying twice with 100 s integration time was used to perform Raman spectroscopy study. SEM images of the cells interspersed with gold nanoclusters immobilized on an indium-tin oxide (ITO) glass substrate were taken on a field-emission scanning electron microscope (Zeiss, Ultra Plus). A JEM-2100 transmission electron microscope (TEM) was used to characterize the size and size distribution of *in situ* biosynthesized gold nanoclusters, which were obtained from the cells by a repetitive freeze-thaw method. The valence state of gold atoms in the *in situ* biosynthesis gold nanoclusters was investigated by a PHI 5000 VersaProbe X-ray photoelectron spectrometer.

Construction of the xenograft tumor mouse model. Three-week-old BALB/c athymic nude mice were purchased from Peking University Health Science Center. All experiments involving mice were approved by the National Institute of Biological Science and Animal Care Research Advisory Committee of Southeast University, while experiments conducted following the guidelines of the Animal Research Ethics Board of Southeast University. All animals were maintained in a specific pathogen free (SPF) house at 24 ± 2°C with a standard 12-hour light/12-hour dark cycle. The animals were allowed free access to tap water and food in the form of a standard pellet diet. Subcutaneous tumor models were generated by the subcutaneous inoculation (0.10 mL volume containing 5×10^7 cells/mL media) of HepG2 cells or K562 cells in the right side of their abdomen using a 1-mL syringe with a 25G needle. Tumor growth was monitored until a palpable size of about 1.0 cm in length was reached in any direction.

Cell and *in vivo* bio-imaging study. For cellular imaging, HepG2, K562 or L02 cells were treated with $HAuCl_4$ solutions and incubated at 37°C for 24 h or 48 h. The cells were washed three times with PBS before fluorescence imaging. A 488-nm excitation laser beam (Andor Revolution XD) was focused using a 20 × IR coated objective (Nikon).

For *in vivo* bio-imaging of gold nanoclusters in the tumor location, the xenograft tumor mice received a subcutaneous injection of 10 mmol/L $HAuCl_4$ solution prepared in PBS (0.1 mL) near the tumor location. The animals were fully anesthetized by inhalation of a mixture of oxygen with 5% isoflurane 24 h or 72 h after the injection. The *in vivo* bio-images were acquired using an *in vivo* fluorescence imaging system (Cambridge Research & Instrumentation, Inc., Maestro EX). The studies were approved by the National Institute of Biological Science and Animal Care Research Advisory Committee of Southeast University, while experiments conducted following the guidelines of the Animal Research Ethics Board of Southeast University.

1. Jiang, S., Gnanasammandhan, M. K. & Zhang, Y. Optical imaging-guided cancer therapy with fluorescent. *J. R. Soc. Interface.* **7**, 3–18 (2010).
2. Gao, X. H., Cui, Y. Y., Levenson, R. M., Chung, L. W. K. & Nie, S. M. *In vivo* cancer targeting and imaging with semiconductor quantum dots. *Nat. Biotechnol.* **22**, 969–976 (2004).
3. Weissleder, R. & Pittet, M. J. Imaging in the era of molecular oncology. *Nature* **452**, 580–589 (2008).
4. Zhao, W. *et al.* Cell-surface sensors for real-time probing of cellular environments. *Nat. Nanotechnol.* **101**, 524–531 (2011).
5. Harada, H. *et al.* Cancer cells that survive radiation therapy acquire HIF-1 activity and translocate towards tumour blood vessels. *Nat. Commun.* **3**, **783**, 1–10 (2012).
6. Zimmer, J. P. *et al.* Size series of small indium arsenide-zinc selenide core-shell nanocrystals and their application to *in vivo* imaging. *J. Am. Chem. Soc.* **128**, 2526–2527 (2006).
7. Shegai, T., Chen, S., Miljković, V. D., Zengin, G., Johansson, P. & Käll, M. A bimetallic nanoantenna for directional colour routing. *Nat. Commun.* **2**, **481**, 1–6 (2011).
8. Chatterjee, D. K., Rufalhah, A. J. & Zhang, Y. Upconversion fluorescence imaging of cells and small animals using lanthanide doped nanocrystals. *Biomaterials.* **29**, 937–943 (2008).
9. Wang, C. S. *et al.* Gold nanoclusters and graphene nanocomposites for drug delivery and imaging of cancer cells. *Angew. Chem. Int. Ed.* **50**, 11644–11648 (2011).
10. Gautier, C. & Burgi, T. Chiral inversion of gold nanoparticles. *J. Am. Chem. Soc.* **130**, 7077–7084 (2008).
11. Román-Velázquez, C. E., Noguez, C. & Garzón, I. L. Circular dichroism simulated spectra of chiral gold nanoclusters: a dipole approximation. *J. Phys. Chem. B.* **107**, 12035–12038 (2003).
12. Peyser, L. A., Vinson, A. E., Bartko, A. P. & Dickson, R. M. Photoactivated fluorescence from individual silver nanoclusters. *Science.* **291**, 103–106 (2001).
13. Yang, Y. & Chen, S. Surface manipulation of the electronic energy of subnanometer-sized gold clusters: an electrochemical and spectroscopic investigation. *Nano Lett.* **3**, 75–79 (2003).
14. Zheng, J. & Dickson, R. M. Individual water-soluble dendrimer-encapsulated silver nanodot fluorescence. *J. Am. Chem. Soc.* **124**, 13982–13983 (2002).
15. Hvkkinen, H. *et al.* Electronic, and impurity-doping effects in nanoscale chemistry: supported gold nanoclusters. *Angew. Chem. Int. Ed.* **42**, 1297–1300 (2003).
16. Crespo, P. *et al.* Permanent magnetism, magnetic anisotropy, and hysteresis of thiol-capped gold nanoparticles. *Phys. Rev. Lett.* **93**, 0872041–0872044 (2004).
17. Balaban, R. S., Nemoto, S. & Finkel, T. Mitochondria, oxidants, and aging. *Cell.* **120**, 483–495 (2005).
18. Zhang, K. & Kaufman, R. J. From endoplasmic-reticulum stress to the inflammatory response. *Nature* **454**, 455–462 (2008).
19. Lim, C. K. *et al.* Chemiluminescence-generating nanoreactor formulation for near-infrared imaging of hydrogen peroxide and glucose level *in vivo*. *Adv. Funct. Mater.* **20**, 2644–2648 (2010).
20. Joerger, R., Klaus, T. & Granqvist, C. G. Biologically produced silver-carbon composite materials for optically functional thin-film coatings. *Adv. Mater.* **12**, 407–409 (2000).
21. Kowshik, M. *et al.* Extracellular synthesis of silver nanoparticles by asilver-tolerant yeast strain MKY3. *Nanotechnology.* **14**, 95–100 (2003).
22. Mandal, D. *et al.* The use of microorganisms for the formation of metal nanoparticles and their application. *Appl. Microbiol. Biotechnol.* **69**, 485–492 (2006).
23. Armendariz, V., Herrera, I., Peralta-Videa, J. R. & Jose-Yacaman, M. Size controlled gold nanoparticle formation by Avena sativa biomass: use of plants in nanobiotechnology. *J. Nanoparticle Res.* **6**, 377–382 (2004).
24. Sharma, N. C. *et al.* Synthesis of plant-mediated gold nanoparticles and catalytic role of biomatrix-embedded nanomaterials. *Environ. Sci. Technol.* **41**, 5137–5142 (2007).
25. Vilchis-Nestor, A. R. *et al.* Solventless synthesis and optical properties of Au and Ag nanoparticles using Camellia sinensis extract. *Mater. Lett.* **62**, 3103–3105 (2008).
26. Kasthuri, J., Veerapandian, S. & Rajendiran, N. Biological synthesis of silver and gold nanoparticles using apiin as reducing agent. *Colloids Surf. B* **68**, 55–60 (2009).
27. Habeeb Muhammed, M. A. *et al.* Bright, NIR-Emitting Au23 from Au25: characterization and applications including biolabeling. *Chem. Eur. J.* **15**, 10110–10120 (2009).
28. Jaramillo, T. F., Baeck, S.-H., Cuenya, B. R. & McFarland, E. W. Catalytic activity of supported Au nanoparticles deposited from block copolymer micelles. *J. Am. Chem. Soc.* **125**, 71485–7149 (2003).
29. Lin, C. A. J. *et al.* Synthesis, characterization, and bioconjugation of fluorescent gold nanoclusters toward biological labeling applications. *ACS Nano.* **3**, 395–401 (2009).
30. Vrana, O. & Brabee, V. Raman spectroscopy of DNA modified by intrastrand cross-links of antitumor cisplatin. *J. Struct. Biol.* **159**, 1–8 (2007).
31. Stone, N., Kendall, C., Smith, J., Crow, P. & Barr, H. Raman spectroscopy for identification of epithelial cancers. *Faraday Discuss.* **126**, 141–157 (2004).

32. Bandekar, J. & Krimm, S. Vibrational analysis of peptides, polypeptides, and proteins. VI. assignment of β-Turn modes in insulin and other proteins. *Biopolymers.* **19**, 31–36 (1980).
33. Szatrowski, T. P. & Nathan, C. F. Production of large amounts of hydrogen peroxide by human tumor cells. *Cancer Res.* **51**, 794–798 (1991).
34. Chang, H. C. *et al*. Layer-by-layer assembly of graphene, Au and poly(toluidine blue O) films sensor for evaluation of oxidative stress of tumor cells elicited by hydrogen peroxide. *Biosens. Bioelectron.* **41**, 789–794 (2013).
35. Amatore, C., Arbault, S., Guile, M. & Guile, M. Electrochemical monitoring of single cell secretion: vesicular exocytosis and oxidative stress. *Chem. Rev.* **108**, 2585–2621 (2008).
36. Zayats, M., Baron, R., Popov, I. & Willner, I. Biocatalytic growth of Au nanoparticles: from mechanistic aspects to biosensors design. *Nano Lett.* **5**, 21–25 (2005).
37. Wiseman, H. & Halliwell, B. Damage to DNA by reactive oxygen and nitrogen species: role in inflammatory disease and progression to cancer. *Biochem. J.* **313**, 17–29 (1996).
38. Trachootham, D., Alexandre, J. & Huang, P. Targeting cancer cells by ROS-mediated mechanisms: a radical therapeutic approach? *Nat. Rev. Drug Discov.* **8**, 579–591 (2009).
39. Bienert, G. P., Schjoerring, J. K. & Jahn, T. P. Membrane transport of hydrogen peroxide. *Biochim. Biophys. Act –Biomembranes* **1758**, 994–1003 (2006).
40. Konishi, Y. *et al*. Intracellular recovery of gold by microbial reduction of $AuCl_4^-$ ions using the anaerobic bacterium Shewanella algae. *Hydrometallurgy.* **81**, 24–29 (2006).
41. Husseiny, I. M., El-Aziz, A. M., Badr, Y. & Mahmoud, A. M. Biosynthesis of gold nanoparticles using Pseudomonas aeruginosa. *Spectrochim. Acta A* **67**, 1003–1006 (2007).
42. Mannervik, B. The enzymes of glutathione metabolism: an overview. *Biochem. Soc. Trans.* **15**, 717–718 (1987).
43. Scott, D., Toney, M. & Muzikar, M. Harnessing the mechanism of glutathione reductase for synthesis of active site bound metallic nanoparticles and electrical connection to electrodes. *J. Am. Chem. Soc.* **130**, 865–874 (2008).
44. Minchimton, A. I. & Tannock, I. F. Drug penetration solid tumor microenvironment. *Nat. Rev. Cancer.* **6**, 583–592 (2006).

Acknowledgements

This work is supported by the National Basic Research Program of China (No.2010CB732404), National Natural-Science Foundation of China (21175020, 90713023), National High Technology Research and Development Program of China (2007AA022007), Doctoral Fund of Ministry of Education of China (20090092110028). In Paris this work was supported by UMR 8640 (ENS-CNRS-UPMC).

Author contributions

J.L.W., C.A. and X.M.W. co-wrote the paper, conducted theoretical analysis, and conceived and designed the experiments. J.L.W., Q.W.L. and H.J. performed the experiments and analyzed the data. G.Z. and C.Y.L. were involved in part of the construction of the xenograft tumor mouse model. All authors contributed to the scientific discussion and revision of the article.

Additional information

Supplementary information accompanies this paper at http://www.nature.com/scientificreports

Competing financial interests: The authors declare no competing financial interests.

How to cite this article: Wang, J. *et al*. *In vivo* self-bio-imaging of tumors through *in situ* biosynthesized fluorescent gold nanoclusters. *Sci. Rep.* **3**, 1157; DOI:10.1038/srep01157 (2013).